Ninth International Conference on CFD in the Minerals and Process Industries
CSIRO, Melbourne, Australia
10-12 December 2012

COMPARISON OF RESOLVED AND COARSE GRAIN DEM MODELS FOR GAS FLOW THROUGH PARTICLE BEDS

James E. HILTON[1*] and Paul W. CLEARY[1]

[1] CSIRO Mathematics, Informatics and Statistics, Clayton, Victoria 3169, AUSTRALIA
*Corresponding author, E-mail address: james.hilton@csiro.au

ABSTRACT

The conventional Discrete Element Method (DEM) typically has a one-to-one correspondence between number of particles in the simulation, *N*, and the number of particles in the system being simulated, *n*. However, large scale industrial systems usually involve prohibitively high *n* for a fully resolved simulation. These are then usually modelled with $N << n$, over a limited domain or with a larger particle diameter and the corresponding assumption of scale invariance. These assumptions are, however, especially problematic in systems where granular material interacts with gas flow, as the dynamics of the system depends heavily on *n*. This has led to a number of suggested modifications for coupled gas-grain DEM to effectively increase the number of particles being simulated. One such approach is for each simulated particle to represent a cluster of smaller particles and to re-formulate the DEM based on these clusters. This, known as a 'coarse grain' method, potentially emulates simulations with $N \sim n$ for low computational cost. We investigate the effectiveness of this coarse grain approach for gas flow through particle beds using resolved and coarse grain models with the same effective particle numbers. The pressure drop and fluidisation characteristics in the beds are measured and compared, and the relative saving in computational cost is weighed against the effectiveness of the coarse grain approach.

INTRODUCTION

The rapid and accurate simulation of coupled gas-grain system has become increasingly important from an industrial perspective for modelling applications such as fluidised beds, pneumatic conveyers, die filling and raceway formation. Popular approaches for computational methods include two-fluid methods, in which the particle phase is represented as an incompressible fluid with a specialised stress-strain relation, and coupled discrete element (DEM) and CFD methods, in which the motion of each particle is simulated using the DEM, coupled by drag relations to a background fluid flow field. Although two-phase methods are fast and effective at capturing fluidisation dynamics, computational resolution can limit the resolvable small scale particle flow structures (van der Hoef *et al.* 2006). Coupled DEM and CFD methods work at a granular level, and are capable of resolving the motion of each grain within the system. This ability makes them exceptionally powerful for resolving the granular dynamics over all length scales within the system. Such detail, however, comes at a computational cost which scales as O(*N*), where *N* is the number of simulated particles in the system. As most industrial systems of interest contain many more particles than are able to be simulated within reasonable timeframes a number of methods to reduce *N* are usually applied in simulations. These include reduction in the geometric volume modelled and/or application of periodic boundary conditions, to exploit symmetries within the system being modelled, restriction of particle sizes, such as omitting fine particles, and application of algorithms to capture the dynamics of sub-resolution scale particles. Of the last of these, the most interesting are representative particle models, in which one 'coarse scale' DEM particle represents a collection of actual 'fine scale' particles in the simulation. A schematic diagram of this method is shown in two dimensions in Fig. 1, where the dashed circle represents a coarse scale particle made up of a number of fine scale particles.

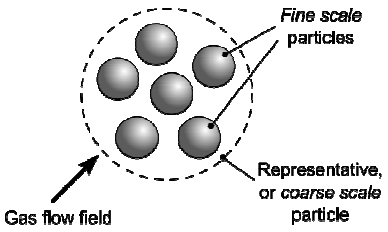

Figure 1: A coarse scale particle representing a collection of fine scale particles.

For large systems of particles it is computationally unfeasible to run a DEM simulation with $N = n$. Such representative particle methods, however, allow the number of fine scale particles N^f to be equal to *n*, where a smaller, computationally feasible, number of coarse scale particles, N^c, are actually used in the DEM simulation. Let:

$$N^f = \kappa N^c \tag{1}$$

where κ is the number of fine scale particles within a coarse scale particle. The ratio κ is chosen to be equal to the ratio of coarse and fine scale particle volumes, such that:

$$\kappa = \frac{V^c}{V^f} = \left(\frac{d^c}{d^f}\right)^3 \tag{2}$$

where *V* is the particle volume and *d* the particle diameter and, throughout, we employ the superscript *c* to represent a coarse scale variable and f to represent a fine scale particle. Let:

$$s = \frac{d^c}{d^f} \tag{3}$$

where the scaling factor $s = \kappa^{\frac{1}{3}}$ is chosen for the simulation. This gives Eq. (1) as:

$$N^c = \frac{N^f}{s^3} \quad (4)$$

This dependence of N^c on s^{-3} gives representative particle models their strength, as the computational cost scales as $O(s^{-3}n)$.

Such models were first suggested by Kazari et al. (1995). A later development to the model was made by Sakano et al. (2000), in which the coarse scale particle was assumed to be a sphere containing packed fine scale particles in an FCC arrangement. However, this method produced bubbles in fluidised beds smaller than experimentally observed bubbles (Mokhtar *et al.*, 2012). A model called the 'similar particle assembly' (SPA) model has been given by Kuwagi et al. (2004), based on particle scaling arguments. This model has been shown to give similar results for s = 3, 6 in fluidised beds (Mokhtar *et al.*, 2012). Sakai introduced a closely related model called the 'coarse grain model' (CGM) which, additionally, incorporates energy conservation arguments between the coarse particle and group of representative particles (Sakai *et al.* 2009, 2010).

REPRESENTATIVE PARTICLE APPROACH

DEM is a Lagrangian method for modelling the individual trajectories of every particle in a granular system. The equation of motion for a particle in a gas flow field is given by:

$$m\frac{\partial \mathbf{v}}{\partial t} = \mathbf{F}_c + \mathbf{F}_d + \mathbf{F}_p + m\mathbf{g} \quad (5)$$

where m is the particle mass, $\mathbf{v}$ the velocity, $\mathbf{F}_c$ the collisional forces, $\mathbf{F}_d$ the drag force, $\mathbf{F}_p$ the force from the gas pressure gradient over the particle, and $\mathbf{g}$ the gravitational acceleration. DEM calculates the collisional forces, $\mathbf{F}_c$, and performs a discrete time-integration of Eq. (5) to give the particle velocities and positions at the next timestep. In systems with gas flow a CFD method is used to calculate the gas flow through a granular media. The CFD and DEM methods are calculated using drag relations, which give $\mathbf{F}_d$ and $\mathbf{F}_p$.

The collisional force is composed of the normal collisional force, $\mathbf{F}_n$, and the tangential collisional force, $\mathbf{F}_t$, acting on the particle, $\mathbf{F}_c = \mathbf{F}_n + \mathbf{F}_t$. These force components act along the normal and in the tangent plane at the contact point, respectively. The magnitude of the normal force is given by a linear-spring dashpot model:

$$F_n = C_n v_n - k_n \delta l \quad (6)$$

where k_n is a spring stiffness, C_n is the normal damping coefficient, which gives a required coefficient of restitution, and v_n is the relative normal speed. The magnitude of the tangential force is calculated incrementally using:

$$F_t = min\left\{\begin{matrix}\mu F_n \\ C_t v_t + k_t \sum v_t \Delta t\end{matrix}\right\} \quad (7)$$

where μ is the Coulomb coefficient of friction, k_t a tangential spring stiffness, v_t the relative tangential velocity, Δt the time-step and C_t a tangential damping coefficient. The incremental sum is taken over the duration of the contact, and models the tangential elastic deformation of the surface, limited by the Coulomb friction μF_n, acting in the direction opposing the applied force.

The gas-particle drag force is given by:

$$\mathbf{F}_d\{d\} = \tfrac{1}{2} C_d\{d\} A \rho_g |\mathbf{u}_r|^2 \hat{\mathbf{u}}_r \quad (8)$$

where C_d is the drag coefficient for a particle of diameter d, A the cross sectional area projected in the direction of the gas flow field, ρ_g the gas density, and $\mathbf{u}_r$the relative gas-particle velocity, where a normal is represented by the circumflex. The drag coefficient C_d is a strong function of both the local bed porosity and the Reynolds number. The gas pressure gradient force is given by:

$$\mathbf{F}_p = V_p \nabla p \quad (9)$$

where V_p is the particle volume and p the gas pressure.

Representative particle approaches are derived by Sakai *et al.* (2010) and Mokhtar *et al.* (2012) using the following approach. First, the equation of motion for a fine scale particle is considered, given by Eq. (5):

$$m^f \frac{\partial \mathbf{v}^f}{\partial t} = m^f \mathbf{g} + \mathbf{F}_n^f + \mathbf{F}_t^f + \mathbf{F}_d^f\{d^f\} + \mathbf{F}_p^f \quad (10)$$

Taking the sum of both sides over the number of particles in a coarse scale particle, κ, gives:

$$\begin{aligned} m^f \sum_\kappa \frac{\partial \mathbf{v}^f}{\partial t} = \\ \kappa m^f \mathbf{g} + \sum_\kappa \left(\mathbf{F}_n^f + \mathbf{F}_t^f + \mathbf{F}_d^f\{d^f\} + \mathbf{F}_p^f\right) \end{aligned} \quad (11)$$

where it is assumed that the mass of all the fine scale particles within the coarse scale particle are the same. The velocities of the fine scale particles are also assumed to be identical and equal to the velocity of the coarse scale particle. This is set to be the average velocity of the fine scale particles:

$$\mathbf{v}^c = \frac{1}{\kappa}\sum_\kappa \mathbf{v}^f \quad (12)$$

From Eq. (11) this gives:

$$m^c \frac{\partial \mathbf{v}^c}{\partial t} = m^c \mathbf{g} + \sum_\kappa \left(\mathbf{F}_n^f + \mathbf{F}_t^f + \mathbf{F}_d^f\{d^f\} + \mathbf{F}_p^f\right) \quad (13)$$

as $\kappa m^f = m^c$. Each of the summations on the right-hand side of Eq. (13) are now considered in turn.

Coarse grain normal Collisional Force

For collisional forces, the coarse grain is assumed to act as a linear superposition of collisions of fine grain particles. Eq. (6) gives:

$$\sum_\kappa F_n^f = C_n^f \sum_\kappa v_n^f - k_n^f \sum_\kappa \delta l^f \quad (14)$$

From Eq. (12) all the normal velocities are identical. Making the further assumption that the coarse scale overlap is the average of the fine scale overlaps gives:

$$\sum_\kappa F_n^f = \kappa\left(C_n^f v_n^c - k_n^f \delta l^c\right) \quad (15)$$

Setting the coarse scale particle normal damping and spring stiffness as:

$$\begin{aligned} C_n^c &= \kappa C_n^f \\ k_n^c &= \kappa k_n^f \end{aligned} \quad (16)$$

gives:

$$\sum_{k} F_n^f = C_n^c v_n - k_n^c \delta l = F_n^c \tag{17}$$

Coarse grain tangential Collisional Force

Using the same assumptions as for the normal force, the representative approach gives the coarse grain tangential collisional force, Eq. (7), as:

$$\sum_{\kappa} F_t^f = min\begin{Bmatrix} \mu \sum_{\kappa} F_n^f \\ \kappa\left(C_t^f v_t + k_t^f \sum v_t \Delta t\right) \end{Bmatrix} \tag{18}$$

where a tenuous assumption has been made that the vectorial sum of the fine grain sliding contacts is equal to the coarse grain sliding contact. From Eq. (17), this becomes:

$$\sum_{\kappa} F_t^f = min\begin{Bmatrix} \mu F_n^c \\ \kappa\left(C_t^f v_t + k_t^f \sum v_t \Delta t\right) \end{Bmatrix} \tag{19}$$

Setting the coarse scale particle tangential damping and spring stiffness as:

$$\begin{aligned} C_t^c &= \kappa C_t^f \\ k_t^c &= \kappa k_t^f \end{aligned} \tag{20}$$

gives:

$$\sum_{\kappa} F_t^f = min\begin{Bmatrix} \mu F_n^c \\ C_t^c v_t + k_t^c \sum v_t \Delta t \end{Bmatrix} = F_t^c \tag{21}$$

Drag force

The drag force is given by Eq. (8). Summation over κ gives:

$$\sum_{\kappa} \mathbf{F}_d^f\{d^f\} = \tfrac{1}{2}\rho_g |\mathbf{u}_r|^2 \hat{\mathbf{u}}_r C_d\{d^f\} \sum_{\kappa} A^f \tag{22}$$

where $C_d\{d^f\}$ indicates that the drag coefficient is calculated using the fine scale particle diameter. For spherical particles and using Eqs. (2, 3), this gives the area summation as:

$$\sum_{\kappa} A^f = \kappa^{\frac{1}{3}} A^c \tag{23}$$

As the coarse scale drag force is given by:

$$\mathbf{F}_d^c\{d\} = \tfrac{1}{2}\rho_g |\mathbf{u}_r|^2 \hat{\mathbf{u}}_r C_d\{d\} A^c \tag{24}$$

The drag expression, Eq. (22) becomes:

$$\sum_{\kappa} \mathbf{F}_d^f\{d^f\} = \kappa^{\frac{1}{3}} \mathbf{F}_d^c\{d^f\} \tag{25}$$

Pressure gradient force

The summation over the pressure gradient force, Eq. (9):

$$\sum_{\kappa} \mathbf{F}_p^f = \nabla p \sum_{\kappa} V_p^f \tag{26}$$

straightforwardly becomes, from Eq. (2):

$$\sum_{\kappa} \mathbf{F}_p^f = \kappa \nabla p V_p^f = \nabla p V_p^c \tag{27}$$

Comparison of equations of motion

In the representative particle approach, the equation of motion, Eq. (13), therefore becomes:

$$m^c \frac{\partial \mathbf{v}^c}{\partial t} = m^c \mathbf{g} + \mathbf{F}_n^c + \mathbf{F}_t^c + \kappa^{\frac{1}{3}} \mathbf{F}_d^c\{d^f\} + \mathbf{F}_p^c \tag{28}$$

where Eqs. (17, 21, 25 and 27) have been used. Comparison of Eq. (28) to the corresponding motion for a fine scale grain, Eq. (13), shows that the *equations of motions for the fine and coarse scale grains are identical,* apart from the drag term. The sub-scale dependency on the gas flow from the finer-scale granular material therefore acts entirely through this drag term. This result is due to inherent assumptions in the model, namely, equating the coarse grain overlap and relative velocities with the sub-cluster average fine particle overlap and their average relative velocities. These are strong assumptions, the consequences of which have not been evaluated to date.

The equations of motion given here are the same as the SPA model (Mokhtar *et al.*, 2012) and the CGM method (Sakai *et al.* 2010). The SPA method appears to have equal damping and spring stiffness in both the normal and tangential directions for both coarse and fine scale particles. Such an approach is allowable as the spring stiffness can be freely chosen and C_n is calculated by the DEM to give a required coefficient of restitution. In the investigation carried out by Mokhtar *et al.*, (2012) the highest value of s is 6, giving $\kappa = 216$. Setting $k_n^c = k_n^f$ rather than $k_n^c = \kappa k_n^f$ would therefore make only a slight difference to the observed maximum particle overlap.

The CGM additionally uses an assumption that each of the fine scale particles are rotating around their individual centres of mass. This assumption leads to the inclusion of a scaling term in the equation for rotational motion. Here, we make the assumption that the moment balance on the collection of fine scale particles is identical to that of the coarse scale particle. This appears to be the same assumption used in the SPA model.

Analytical test of a falling particle

As an initial test case we consider the simplest possible gas-grain system: a single particle freely falling in a gas. Both a single particle of diameter d^f and a cluster of particles of diameter d^f represented by a coarse particle of diameter d^c should fall at the same velocity. From Eqs. (8 and 10), neglecting the pressure gradient, the equation of motion for a particle of diameter d^f falling in a gas with a vertical velocity v_y is:

$$\frac{\partial v_y}{\partial t} - C_d\{d^f\} \frac{A^f \rho_g}{2m^f} v_y^2 - g = 0 \tag{29}$$

which, for a spherical particle, reduces to:

$$\frac{\partial v_y}{\partial t} - \tfrac{3}{4} C_d\{d^f\} \frac{1}{d^f} \frac{\rho_g}{\rho} v_y^2 - g = 0 \tag{30}$$

the solution to which has the form $v_y \propto \tanh(t)$. For a coarse grain particle, Eqs. (24 and 28) give:

$$\frac{\partial v_y}{\partial t} + \kappa^{\frac{1}{3}} C_d\{d^f\} \frac{A^c \rho_g}{2m^c} v_y^2 - g = 0 \tag{31}$$

which reduces to:

$$\frac{\partial v_y}{\partial t} + \tfrac{3}{4} C_d\{d^f\} \frac{\kappa^{\frac{1}{3}}}{d^c} \frac{\rho_g}{\rho} v_y^2 - g = 0 \tag{32}$$

But, as $\kappa^{\frac{1}{3}} d^f = d^c$, Eq. (32) is exactly the same equation of motion as Eq. (30). Therefore both the fine scale particle and collection of fine scale particles represented by a coarse scale particle fall at the same rate. For this simple analytic case the representative particle model therefore gives a correct result.

IMPLEMENTATION

The analysis carried out in the previous section has shown that a representative particle model can be implemented with great simplicity in a coupled DEM/CFD formulation, as only the drag term differs between fine and coarse scale models. The steps to modify the formulation are as follows:

1. Choose a coarse grain diameter, d^c, which represents a collection of finer particles of diameter d^f.
2. When calculating the drag force, use the drag coefficient for d^f, $C_d\{d^f\}$.
3. Multiply the drag force by $s = \kappa^{\frac{1}{3}} = d^c/d^f$ and apply to the particles.

All calculations in the DEM method use the coarse grain diameter d^c, apart from the drag term, which is calculated as described.

In our implementation the CFD component of the model is based on the constitutive equations for fluid, or gas, flow through a porous bed, formulated such that the interstitial flow is assumed incompressible. The method is covered in detail in Hilton *et al.*, (2010), and has been applied to numerous gas-grain systems, including pneumatic conveying (Hilton and Cleary 2011) and raceway formation (Hilton and Cleary 2012).

Computational modelling of a fluidised bed

A model of a fluidised bed was used to compare the representative particle method to fully resolved simulations. The bed contained spherical particles of varying diameter and different gas flow velocities. The set-up used is shown schematically in Fig. 2. A uniform inflow with gas velocity v_y was applied over the base of the particle bed, with an identical outflow over the top of the domain. The domain was filled by creating particles over a regular grid at the top of the domain and allowing them to freely fall under gravity until $\frac{2}{3}$ of the domain by height had been filled. The boundary conditions in the *x* and *z* directions were solid walls, with a no-slip zero velocity boundary condition applied for gas.

The parameters used in the simulations are given in Table 1. Each simulation was run for a total of 2 s. The grid resolution in the *x*, *y* and *z* directions was $10 \times 30 \times 10$, giving a grid resolution of 10.2 mm.

Parameter		Value
Particle density	ρ_p	1000 kg/m^3
Gas density	ρ_g	1.2 kg/m^3
Gas viscosity	η	1.8×10^{-5} Pa s
Particle friction	μ	0.1
Spring stiffness	k	1.0×10^4 N/m
Coefficient of restitution	e	0.5

Table 1: Simulation parameters used

The inflow gas velocity was varied from 0.2 to 2 m/s in increments of 0.2 m/s. Verification of the pressure gradient was carried out by comparing measurements from the simulations to an empirical expression given by Ergun (1952):

$$\frac{\partial p}{\partial y} = \frac{\rho_g v_y^2}{d}\left(\frac{1-\varepsilon_b}{\varepsilon_b^3}\right)\left(\frac{150\eta(1-\varepsilon_b)}{\rho_g v_y d} + 1.75\right) \qquad (33)$$

where ε_b is the bulk packing fraction, calculated from the number of particles multiplied by the volume of each particle divided by the total volume enclosing them. This is slightly different from the bed packing fraction, ε, due to the reduction of the packing fraction from boundary effects near the walls. Fluidisation occurs when the weight of the bed balances the applied pressure gradient. Neglecting wall friction, this is given by:

$$\left(\frac{\partial p}{\partial y}\right)_c = (1-\varepsilon)(\rho_s - \rho_g)g \qquad (34)$$

The inflow gas velocity required to reach this point is the 'lift-off' velocity.

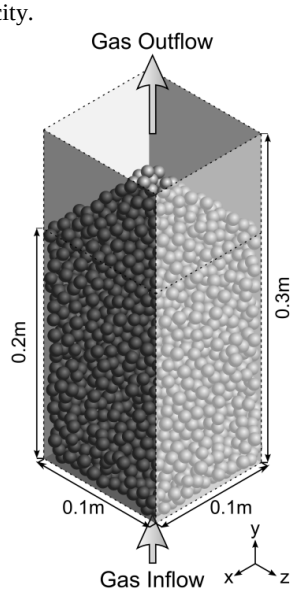

Figure 2: Fluidised bed test case set-up.

Fluidised bed with fully resolved particles

For comparison, the fluidised bed was first simulated for a range of particle diameters, given in Table 2, using a standard coupled DEM-CFD method. These results were then compared to simulations using a representative particle approach. The pressure gradients as a function of inflow velocity are shown in Figs. 3, 4, and 5 for resolved particle diameters of 4 mm, 3 mm and 2 mm respectively. The Ergun equation, Eq. (33) is shown as a dashed curve in each figure, and the error bars shown one standard deviation of the measured pressure gradient within the particle bed. The lift-off pressure gradient is also shown as the horizontal dotted line in each figure.

d	ε	ε_b	N
2 mm	0.626	0.611	291,914
3 mm	0.624	0.604	85,585
4 mm	0.623	0.597	35,640
5 mm	0.620	0.591	18,079
6 mm	0.619	0.587	10,374

Table 2: Particle diameters used with corresponding bed and bulk packing fraction, and number of particles.

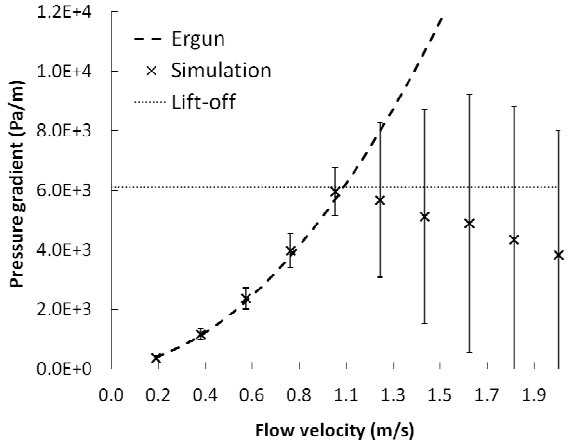

Figure 3: Pressure gradient for $\boldsymbol{d = 4}$ mm particles.

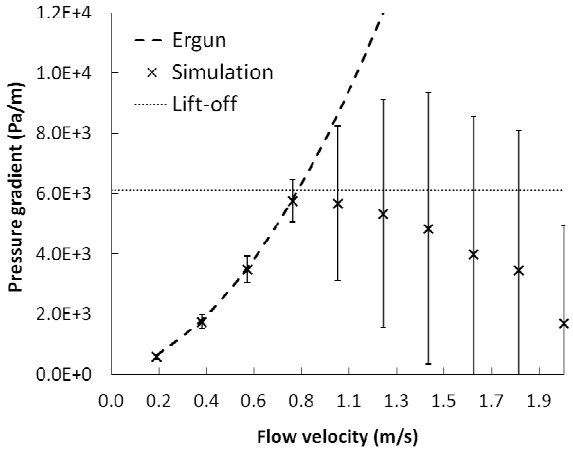

Figure 4: Pressure gradient for $\boldsymbol{d = 3}$ mm particles.

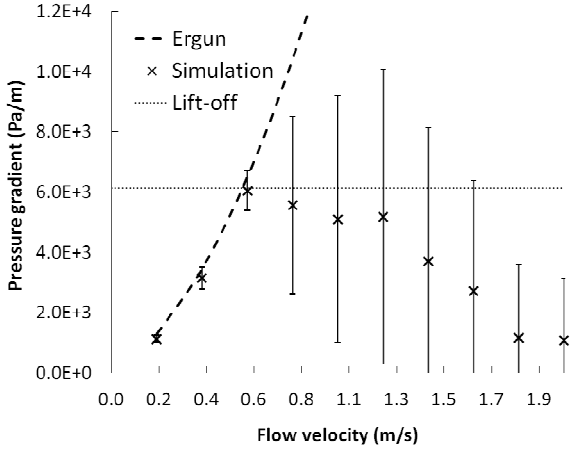

Figure 5: Pressure gradient for $\boldsymbol{d = 2}$ mm particles.

The behaviour of the fluidised bed was exactly as expected, closely following the empirical expression for all particle diameters until the pressure gradient reached the bed weight. At this point the bed fluidised, characterised by a large spread in instantaneous pressure gradient and, visually, by well-known bubbling and slugging characteristics (van der Hoef *et al.* 2006), as shown in Fig. 6 for 2 mm particles. Graphs of diameter 6 mm and 5 mm have been omitted due to space limitations, but show the same behaviour.

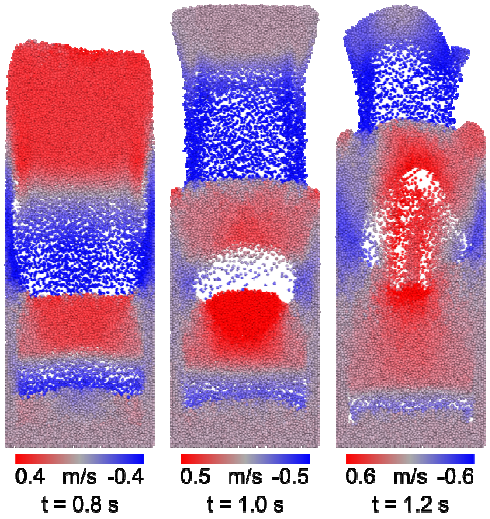

Figure 6: Fluidisation behaviour in a bed with fully resolved particles of diameter 2 mm and an inflow velocity of 1.0 m/s. A cross section over the bed is shown, and the particles are shaded by their velocity in the vertical (y) direction.

Comparison with representative particle model

The representative particle method was used to simulate fine particles of 4, 3 and 2 mm using a coarse grain size of 6 mm. A summary of the parameters used and relative computational time compared to the fully resolved simulations is given in Table 3. As in the study by Mokhtar *et al.*, (2012), the spring stiffness was set to the same value in each simulation, given in Table 1.

d^f	d^c	s	N^f	T/T^{CGM}
2 mm	6 mm	3.0	280,098	68.64
3 mm	6 mm	2.0	82,992	15.73
4 mm	6 mm	1.5	35,012	4.22

Table 3: Parameters for the representative particle simulations. $\boldsymbol{T/T^{CGM}}$ is the ratio of computational time taken for the fully resolved simulation, $\boldsymbol{T}$, to the representative, coarse grain, simulation, $\boldsymbol{T^{CGM}}$.

The pressure gradients for the representative method as a function of inflow velocity are shown in Figs. 7, 8, and 9 for particle diameters with fine grain diameters of 4 mm, 3 mm and 2 mm respectively. Comparison of the results from the fine scale and fully resolved simulations at the same particle diameter show that the fluidisation characteristics match reasonably well, despite the very basic sub-scale drag dependency. The representative particle method also matched the Ergun expression until the lift-off velocity was reached, although small deviation from the empirical curve was found at smaller particle diameters. This deviation appear to grow as s increased, which we attribute to the increasing importance of the absent sub-cluster structure and dynamics. After lift-off the bed showed similar fluidisation characteristics to the fully resolved bed. However, the lift-off point was found to be moderately higher than the empirical expression given by Eq. (34) when using the representative particle approach, as shown by the circled points in Figs. 8 and 9, respectively.

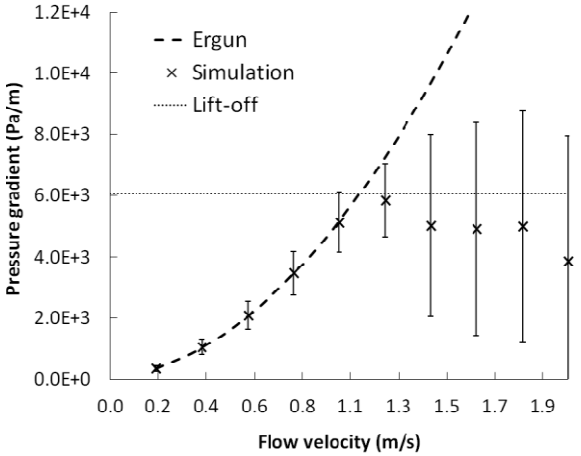

Figure 7 - Pressure gradient for $d^f = 4$ mm particles.

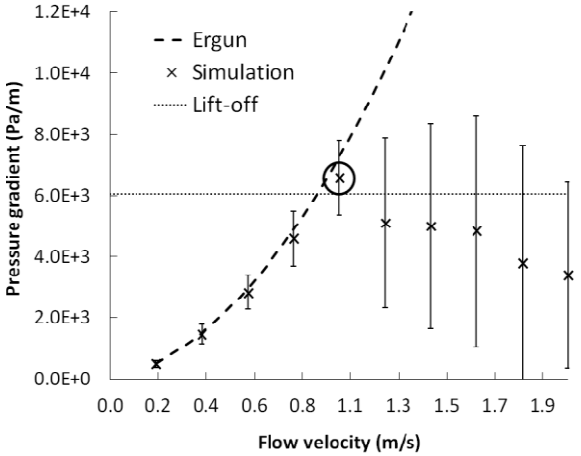

Figure 8 - Pressure gradient for $d^f = 3$ mm particles.

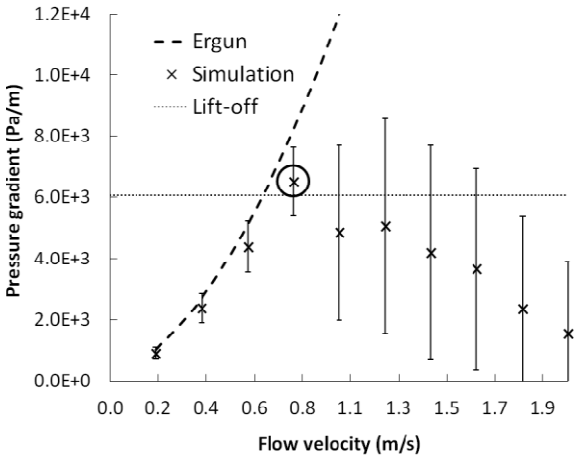

Figure 9- Pressure gradient for $d^f = 2$ mm particles.

Despite the higher transition velocity the overall behaviour of the representative particle method showed surprisingly similar results to the fully resolved method, at a fraction of the computational time. As shown in Table 3, a two second simulation can be completed around 70 times faster than a fully resolved simulation for $d^f = 2$ mm. For moderate scale ratios *s*, the model therefore appears to be able to provide useful computational acceleration with limited loss of accuracy.

CONCLUSION

Fully resolved and representative simulations of fluidised beds with the same fine scale particle diameters show broadly similar pressure and fluidisation characteristics. Deviation from the empirical curve given by the Ergun relation was found for small fine grain diameters. As the maximum ratio used was $s = 3$, more work is required to understand this deviation at larger values of *s*. The bed lift off point was also found to be moderately higher than expected when using the representative model.

Such straightforward fluidised bed simulations have only minor dependence on the system geometry. It is likely that in gas-particle systems dominated by inter-grain or grain-boundary collisions this method may not give the correct dynamics as the DEM component would be limited by the coarse grain size. Examples of such systems include die filling and discharge of fine powders from narrow outlets, both of which are affected by gas, but are also strongly influenced by geometrical factors. Considerable testing is necessary to understand the limitation of this method in relation to such systems.

For fluidised beds, at least, the 'coarse grain' or representative particle approach appears to provide a plausible method to increase the effective number of particles in an extremely straightforward manner. Such coarse grain simulations can be run in a fraction of the time of the fully resolved simulations, and therefore provide a significant computational saving with little overhead. Although such a method could potentially allow industrial systems to be simulated with $N \sim n$, further work must be undertaken to understand the limitations of the model and the many assumptions used to construct it. In particular, the behaviour of the model at high values of the coarse grain scaling factor should be investigated before this can become a viable approach for industrial gas-grain systems.

REFERENCES

Di FELICE, R., (1994), *Int. J. Multiphase Flow*, **20**, 153-159.

ERGUN, S., (1952), *Chem. Eng. Prog.*, **48**, 89-94.

HILTON, J.E., MASON, L.R. and CLEARY, P.W., (2010), *Chem. Eng. Sci.*, **65**, 1584-1596.

HILTON, J.E., and CLEARY, P.W., (2011), *Chem. Eng. Sci.*, **66**, 231-240.

HILTON, J.E., and CLEARY, P.W., (2012), *Chem. Eng. Sci.*, **80**, 306-316.

KAZARI, M., ROKO, K. KAWAGUCHI, T. TANAKA, T. and TSUJI, Y. (1995), *Proc. of 2nd Int.Conference on Multiphase Flow, Kyoto, Japan*, FB2.9–FB2.15

KUWAGI K, TAKEDA H. and HORIO M., (2004), *Int. Conf. on Fluidization Eng. XI, Naples*, 243–250.

MOKHTAR, M. A., KUWAGI, K, TAKAMI, T., HIRANO, H. and HORIO, M. (2012), *A. I. Ch. E.*, **58**, 87-98.

SAKANO M., YASO T. and NAKANISHI H. (2000), *Jpn. J. Multiphase Flow*, **14**, 66–73.

SAKAI M., KOSHIZUKA S., (2009), *Chem. Eng. Sci.*, **64**, 533–539.

SAKAI M., YAMADA Y., SHIGETO Y., SHIBATA K,. KAWASAKI V.M., KOSHIZUKA S. (2010), *Int. J. Numer. Meth. Fluids*, **64**, 1319–1335.

VAN DER HOEF, M.A., YE, M., VAN SINT ANNALAND, M. ANDREWS, IV A.T., SUNDARESAN, S. and KUIPERS, J.A.M. (2006), *Advances in Chemical Engineering*, **31**, 65-149.